

High-order wavefront sensing system for PALM-3000

Christoph Baranec

Caltech Optical Observatories, 1200 E. California Blvd., Pasadena, CA, USA 91125

ABSTRACT

PALM-3000 is an upgrade to the current PALM-241 adaptive optics system at the 5.1 m Hale telescope which will allow diffraction-limited science in visible wavelengths using bright natural guide stars, have more modest performance with an upgraded Sodium laser guide star, and allow for guiding on faint natural guide stars. A key sub-system of the upgrade is a new high-order Shack-Hartmann wavefront sensor with selectable pupil sampling, up to 64 subapertures across the telescope aperture, to minimize wavefront reconstruction error for varying brightness of guide source with a frame rate up to 3 kHz. The design and current status of the high-order wavefront sensing system is presented.

Keywords: adaptive optics, extreme adaptive optics, wavefront sensors

1. INTRODUCTION

PALM-3000 is an upgrade to the current PALM-241 adaptive optics system^{1,2} at the 5.1 m Hale telescope which will allow diffraction-limited science in visible wavelengths using bright natural guide stars, have more modest performance with an upgraded Sodium laser guide star, and allow for guiding on faint natural guide stars. Currently, the system supports the J-, H- and K-band coronagraphic and imaging science instrument PHARO³ and will support two new integral field spectrographs, Oxford SWIFT⁴ for moderate resolution in the red optical bands and P1640⁵ for high-contrast observations in the infrared.

For more details on the PALM-3000 adaptive optics upgrade please see Dekany et al.⁶ and Bouchez et al.⁷. Correction of the wavefront will be accomplished with a woofer-tweeter deformable mirror configuration with both 349 and 3,368 actuator count deformable mirrors. Note that this adaptive optics system will sense and correct higher spatial frequencies than that of the high contrast adaptive optics systems being implemented for Gemini (Gemini Planet Imager)⁸ and the VLT (Spectro-Polarimetry High-contrast Exoplanet Research)⁹. PALM-3000 is predicted to achieve residual wavefront errors of ~ 84 nm RMS with a guide source of $m_V = 7$ in good seeing⁶ ($r_0 = 15$ cm at $\lambda = 500$ nm). High-order wavefront sensing will be done with a Shack-Hartmann wavefront sensor with selectable pupil sampling up to 64 subapertures across the telescope aperture. Additional low-order wavefront sensing will also be accomplished using a 3×3 Shack-Hartmann wavefront sensor when supporting the Sodium laser guide star; later upgrading to a 2×2 Shack-Hartmann sensor for greater signal-to-noise slope measurements enabling the ability to low-order sense on fainter sources. An infrared tip/tilt sensor to increase sensitivity and sky coverage will be implemented approximately one year after initial PALM-3000 operations¹⁰.

The optical and mechanical designs of the high-order wavefront sensor are detailed herein.

2. OPTICAL DESIGN

2.1 Overview and layout

The high-order wavefront sensor is a Shack-Hartmann design with adjustable spatial pupil sampling to minimize wavefront reconstruction error over a wide range of guide star brightness, with the ability to run at frame rates up to 3 kHz. This is necessary to support a broad range of observing scenarios envisioned for the PALM-3000 system^{6,7}. The wavefront sensor is designed to be sensitive over a bandwidth from $\lambda = 400$ to 900 nm and be able to guide on natural guide stars, laser guide stars and other extended sources such as solar system objects. It will be able to select a guide source from anywhere within a 2 arc minute field centered on the telescope's axis. Figure 1 shows an optical layout of the high-order wavefront sensor.

Send correspondence to C. Baranec, E-mail: baranec@astro.caltech.edu

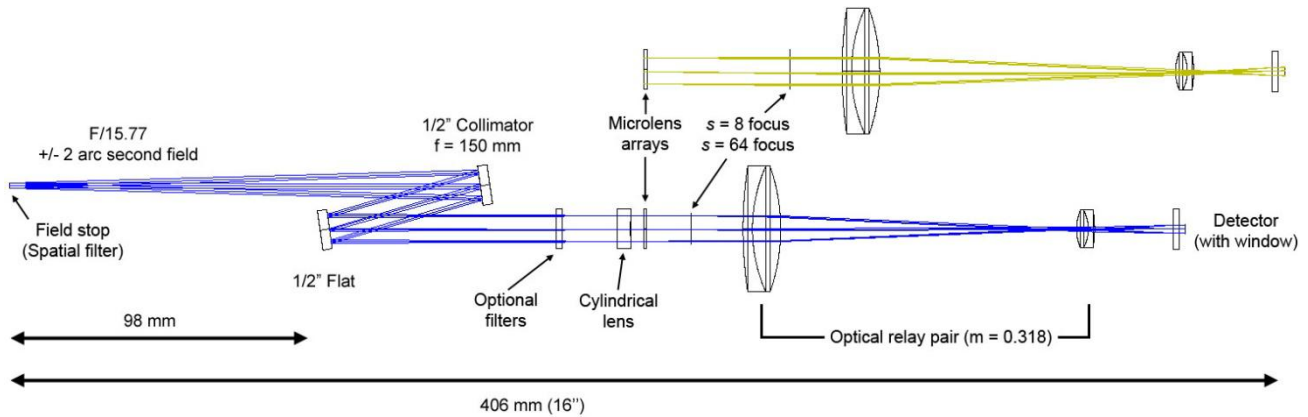


Fig 1. Optical layout of the high-order Shack-Hartmann wavefront sensor for PALM-3000. The lower configuration (blue) shows a 4 arc second field of view, the largest allowed by the spatial filter/ field stop, entering the high-order wavefront sensor. The light is then collimated and the pupil imaged onto the microlens array, with an optional cylindrical lens to remove the static astigmatism error introduced. The $s = 64$ array can be remotely selected among the four arrays ($s = 8$ array shown top; yellow) and focuses the Shack-Hartmann pattern to a focal plane. The detector and relay optics, with a magnification of approximately 0.3, are linked together on a focus stage to accommodate the focal plane shift of the different microlens arrays. The entire sensor package is mounted on a linear stage to change focus between stellar and laser guide sources.

The entrance to the wavefront sensor will be fitted with a field stop that will also function as a spatial filter¹¹. The spatial filter consists of two blades forming a square aperture which can be adjusted remotely in size via a piezo-electric flexure mechanism. An early version of the spatial filter is being constructed for use with the current Palomar adaptive optics system to support observations with the Well-Corrected Subaperture¹² project, which will also be supported in the PALM-3000 upgrade. The spatial filter used in PALM-3000 will have a maximum aperture size of 4 arc sec (1.56 mm) for guiding on solar system objects, and a minimum size of 0.48 arc sec (190 μm) to filter out spatial frequencies above λ/d for the 16 across pupil sampling mode. Support for spatial filtering for the 8 across pupil sampling mode will not be supported because aliasing error will not be the dominant error term in wavefront reconstruction.

The second element in the system is a reflective collimator which images the pupil onto the microlens array. The collimator is reflective to control errors in the pupil size as a function of color over the large bandwidth of the sensor. It also introduces enough astigmatism error to match the geometries of the projected pupil on the deformable mirror to the projected pupil on the microlens array. This will be discussed in more detail in Section 2.2. A flat is included to fold the beam to ease packaging.

The space between the fold flat and microlens array is reserved for a set of optional filters.

Immediately before the microlens array is a cylindrical lens which removes the local tilts from each of the subapertures while still allowing the projected pupil geometries to be matched. This ensures that the spots in the Shack-Hartmann pattern are located at the center of pixel boundaries and do not use up dynamic range on the wavefront sensor.

There are four different microlens arrays which can be selected to be used for wavefront measurement. Each will have different spatial pupil sampling and focal lengths and will be described in more detail in Sections 2.3 and 2.4. The focal planes differ in location up to 12 mm.

Downstream of the microlens arrays are the relay optics and detector. The optics act as a 0.318 demagnification relay to reimaging the spots created by the microlens array to the detector. The detector is an E2V CCD50: a 128 square, 24 μm /pixel split frame transfer CCD with 16 parallel output amplifiers and support for frame rates up to 3 kHz. A chopper to support range gating of the Sodium laser guide star will also be included close to the detector as exists in the current Palomar laser adaptive optics system².

Note that an atmospheric dispersion corrector is being considered upstream of the spatial filter to control the guide source elongation due to the chromatic effects of the atmosphere. If atmospheric dispersion is not controlled at low zenith angles, the spatial filter will selectively clip the low and high ends of the wavelength range.

2.2 Pupil projection

To maintain closed-loop stability and minimum registration error between the deformable mirrors and wavefront sensor, an absolute mismatch tolerance of 10-15% of a subaperture has been adopted in the design, with a tighter 5% stability requirement during an hour long exposure. This tolerance raises two issues, a design to match the pupil size over the wide wavelength range of 400 to 900 nm, and the projection of the pupil on the tilted deformable mirrors.

The first issue can be solved in multiple ways. The longitudinal color of a standard two glass achromatic lens can be controlled only to a level such that the projected pupil on the microlens array would be approximately $\pm 6\%$ in size of the finest subaperture. This essentially means that the projected pupil would consist of different sizes for different colors and would use all of the allowable error. The color correction can be extended by using a custom air spaced triplet that includes the use of a fluoride in addition to the classical crown and flint glasses. This can reduce the mismatch in pupil size to an acceptable $\sim \pm 1\%$ in size of the finest subaperture; however the additional losses due to multiple surface reflections and absorption should be taken into account. Alternatively, a reflective collimator can be used in which case color effects are eliminated.

The use of a reflective collimator also allows for addressing the issue of the projection of the pupil onto the tilted deformable mirrors. In the current PALM-AO system, the angle of incidence of collimated light on the deformable mirror is 7.6° , causing an elliptical projection of the pupil onto the deformable mirror with a major to minor axis ratio of ~ 1.01 . This results in little error in the current wavefront sensor as it is only 16×16 . However with the PALM-3000 upgrade, the two deformable mirrors will most likely be used at higher angles of incidence due to packaging requirements, likely 11.5° to 13° . This, in turn, creates an elliptical projection with an axis ratio of 1.020 to 1.025 which corresponds to roughly one actuator difference in the two axes on the high-order deformable mirror.

To maintain a Fried geometry across the pupil, the pupil should be similarly distorted on the microlens array of the wavefront sensor. This is not absolutely necessary as some adaptive optics systems, eg. MMT¹³, have completely different geometries in terms of sensors and correctors; however a more thorough study of the particular geometries in question, whether or not it is necessary to distort the pupil wavefront sensor, similar to those done for other geometries¹⁴⁻¹⁶ needs to be done.

Again, the pupil distortion required can be achieved in many ways. One option is the use of a tilted off-axis parabola, while possibly expensive to manufacture, has the advantage of also being able to create a circular pupil when not tilted. Another is to use a tilted concave spherical element which has inherent astigmatism. In the design presented in Figure 1, a tilted spherical mirror is used which projects a pupil with a 1.02 major to minor axis ratio on the microlens array. One drawback to distorting the pupil in this way, with either option, is that static astigmatism, on the order of 300 nm RMS, is introduced in the wavefront sensor, causing the edge spots to run off null by $2 \mu\text{m}$ over a 2×2 pixel subaperture which is $48 \mu\text{m}$ on a side. This can be corrected by placing a cylindrical lens near the pupil which leaves only 20 nm RMS of residual coma in the wavefront sensor.

It is the intention to leave the final design of the collimating element flexible for the time being. Initially, the spherical option will be adopted until such time as the design of the relay is finalized in which case the final angle of incidence on the deformable mirrors would be determined. Since there exists uncertainty in the final F/# delivered to the wavefront sensor, the focal length may need to be changed and subsequently spherical mirrors with $< 0.1\%$ tolerance on focal length could be obtained quickly at an economical cost.

2.3 Adjustable pupil sampling

The optimization of pupil sampling, s , in the wavefront sensor which maximizes an adaptive optics system's delivered Strehl ratio is achieved by finding the spatial sampling which reduces the total wavefront reconstruction error. This is the sum in quadrature of pupil sampling dependent error sources, fitting error and measurement error, temporal errors associated with the frame rate. Angel¹⁷ explored the joint optimization of spatial and temporal sampling of a wavefront in regard to high-order extreme adaptive optics systems, but this is extended to a larger range of observing conditions, including the use of dim guide sources. Using expressions for fitting, measurement and time delay error (Hardy¹⁸; eq. 6.36, 5.13, 9.56, 9.58), optimization of s and the frame rate can be determined numerically. Further details on the analysis can be found in Baranec¹⁹.

Figure 2 presents the total wavefront reconstruction error as a function of s where the frame rate has been optimized at each point, for different visual magnitude stars at the Hale telescope under median seeing conditions of $r_0 = 9.2$ cm at $\lambda = 500$ nm. It can be seen that for any given magnitude of guide star, there is an optimal pupil sampling, s_{opt} , which minimizes the wavefront reconstruction error. Table 1 presents s_{opt} and the frame rate, f_{opt} , which minimizes the wavefront reconstruction error, for each magnitude of guide star presented in Figure 1.

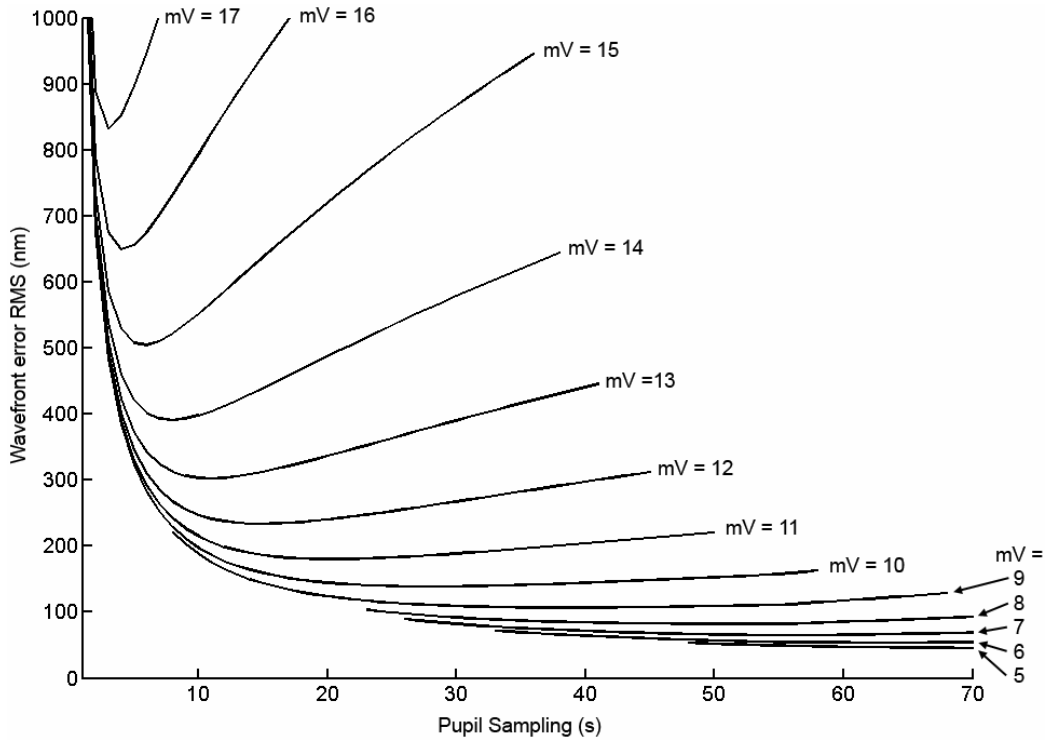


Fig 2. Wavefront reconstruction error as a function of pupil sampling, s , at the 5.1 m Hale telescope. Curves are labeled with the visual magnitude of natural guide star used. All assume a telescope transmission of 24%, typical CCD quantum efficiency, read noise = $5 e^-$, number pixels across a subaperture = 2, $r_0 = 9.2$ cm, and $\tau_0 = 3$ ms with a two frame time delay.

Table 1. Optimal pupil sampling and frame rate as a function of visual magnitude for the 5.1 m Hale telescope. These values correspond to the minima in curves presented in Figure 1.

| m_V | s_{opt} | f_{opt} (fps) | Recon. Error (nm) |
|-------|-----------|--------------------|----------------------|
| 5 | 78 | 3188 | 45 |
| 6 | 63 | 2558 | 54 |
| 7 | 56 | 1847 | 65 |
| 8 | 53 | 1204 | 82 |
| 9 | 38 | 887 | 107 |
| 10 | 28 | 646 | 139 |
| 11 | 20 | 478 | 180 |
| 12 | 15 | 346 | 234 |
| 13 | 11 | 254 | 303 |
| 14 | 8 | 188 | 391 |
| 15 | 6 | 137 | 505 |
| 16 | 4 | 107 | 649 |
| 17 | 3 | 79 | 832 |

Over a range of visual magnitudes from 5 to 15, s_{\min} varies from 6 to 78. For brighter guide sources at higher sampling, there is a shallow minimum of s around s_{\min} ; however for dimmer sources, the necessity to adjust s is apparent as the error curves are more sharply curved. In traditional adaptive optics systems, the spatial sampling of the wavefront is usually fixed, leading to excessive wavefront reconstruction error at anything but a particular intensity of guide star.

This leads to the necessity to have different spatial pupil samplings and frame rates available to the observer. This was identified in the design of the NAOS system where low resolution, 7×7 , and high resolution, 14×14 , sampling of the wavefront supports observing with dimmer and brighter guide stars respectively^{20,21}. The PALM-3000 system will be available to support a wide range of observing modes, and therefore has been chosen to support spatial pupil sampling of 8×8 , 16×16 , 32×32 and 64×64 , with frame rates up to 3 kHz. The factors of two in sampling make it convenient to use the same 128×128 pixel detector for each mode. It is envisioned that a simple tool taking calculations of optimal sampling and frame rates into account will be available to support observations after being verified experimentally.

2.4 Microlens array selection

To support the different pupil sampling modes of the wavefront sensor, four different microlens arrays have been selected. The spot sizes for both natural stars, the sodium laser guide star and solar system objects have been calculated assuming median seeing, $r_0 = 9.2$ cm, and a zenith angle of 30° , including effects from diffraction, aberrations in the wavefront sensor (assuming ~ 0.25 arc sec), and charge diffusion (~ 0.5 pixels). Table 2 lists the expected spot sizes along with the chosen plate scale for each microlens array and the subaperture angular size.

Table 2. Expected spot sizes on the detector for the four different spatial pupil sampling modes and chosen plate scales and subaperture angular sizes. *Example solar system objects include the planets Uranus and Neptune.

| s | spot size (arc sec) | | | Plate scale (arc sec/pixel) | Subap. size (arc sec) |
|-----|---------------------|------|-------------|--------------------------------|--------------------------|
| | NGS | LGS | Solar sys.* | | |
| 64 | 1.8-2.3 | - | - | 2.1 | 4.2 |
| 32 | 1.50 | 2.14 | 3.5/2.7 | 1.5 | 6.0 |
| 16 | 1.33 | 2.04 | - | 1.3 | 10.4 |
| 8 | 1.28 | 2.01 | - | 0.65 | 10.4 |

The spot size for $s = 64$, which will only be used with bright enough natural guide stars ($m_V \sim 5 - 7$), is dominated by diffraction along with possible charge diffusion, and the plate scale was chosen to give a ratio of pixel to spot size of ~ 1 which provides good linearity around the zero-point (Hardy¹⁸; table 5.3) since centroiding is restricted to using only 2×2 pixels. The plate scale for $s = 32$ was chosen again to give good linearity when using only 2×2 pixels in NGS mode; however when guiding on extended objects, the option to use 4×4 pixels, either with a center of mass or correlation tracker, or binned, to an effective plate scale of 3.0 arc sec/pixel, is also available. The same justification applies to the selection of the $s = 16$ plate scale. The $s = 8$ plate scale is a result of a compromise with the imaging performance of the relay optics. To maintain the same pixel to NGS spot size ratio of 1, the F/# of the microlens array would be reduced to the point where aberrations in the relay would be the dominant factor in spot size, increasing centroiding error unnecessarily. To compensate for this, the F/# from the $s = 16$ microlens array is adopted and as a consequence the plate scale for $s = 8$ is finer by a factor of two. This means that the detector will be binned either by 2 for NGS guiding or by 3 for LGS guiding. The $s = 8$ mode will be used primarily for faint NGS or when the Sodium abundance is particularly low, and as such, wavefront measurements will be done in a photon starved regime. In this case, it will be particularly important to control the dark current on the detector by cooling the back end of the CCD thermo-electric cooler appropriately.

2.5 Relay design

The relay system that will image the microlens array focal plane array has been selected as a pair of commercially available achromatic lenses with broadband anti-reflection coatings. The design magnification of 0.318 can be adjusted by $\pm 10\%$ with negligible degradation in image quality. The relay has been designed to accept light from the microlens arrays down to an F/# of approximately 37. Figure 3 shows spot diagrams for a relayed F/37 beam from the center to the edge of the field. Each grid represents 2×2 pixels, $48 \times 48 \mu\text{m}$, on the CCD.

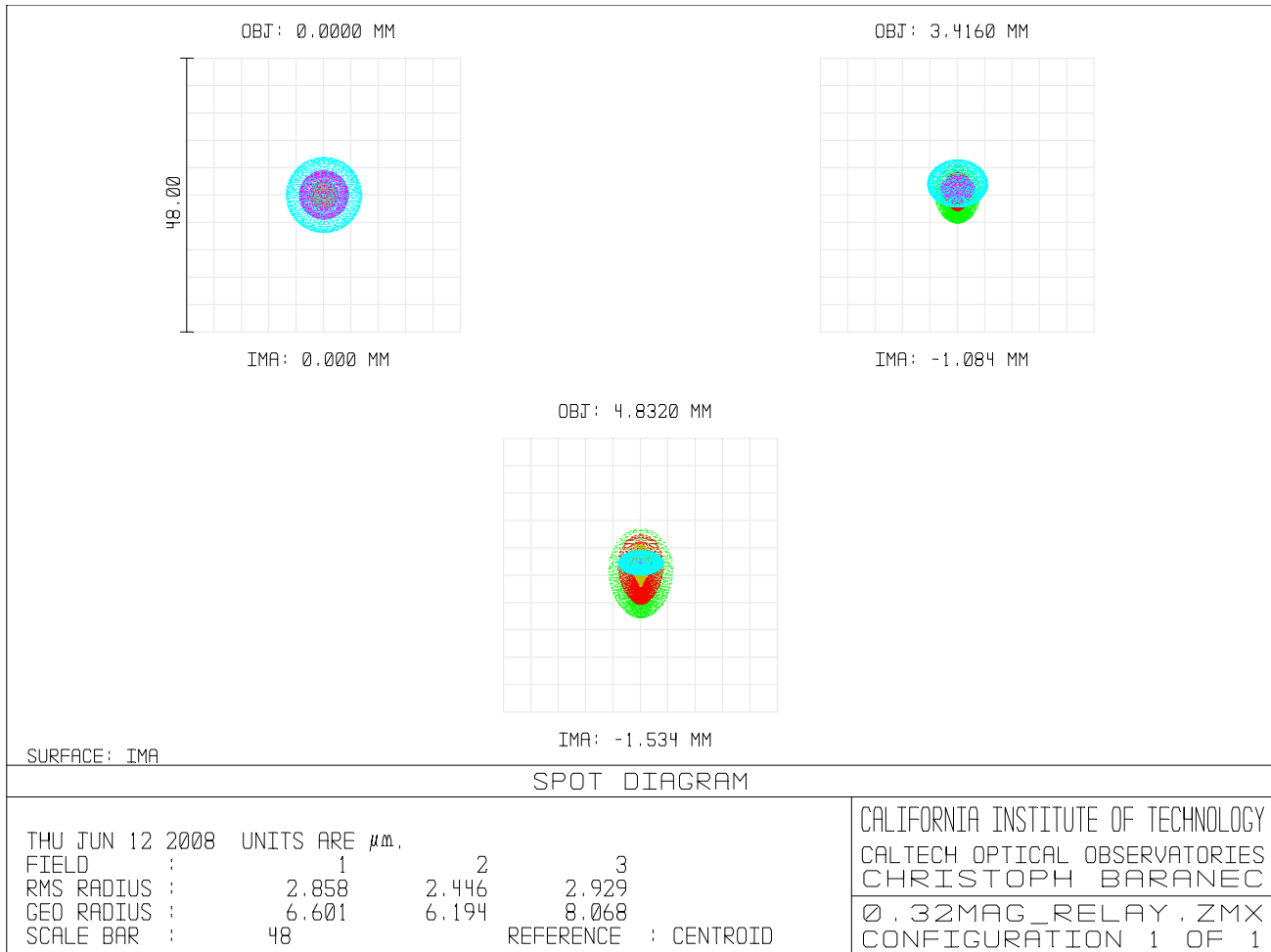


Fig. 3. Spot diagrams from the relay system for an F/37 beam at the center, 0.71 and full field over the full wavelength range of $\lambda = 400 - 900 \text{ nm}$.

RMS spot diameters are smaller than $6 \mu\text{m}$, or a quarter of a pixel, and geometric diameters are less than $16 \mu\text{m}$, or two-thirds of a pixel. The relay also exhibits extremely low distortion, $< 0.002\%$ or $< 0.3 \mu\text{m}$ at the edge of the field.

2.6 End to end optical performance

The imaging performance of the optical design of the high-order wavefront sensor has been analyzed. A Zemax model has been constructed which includes the Hale telescope and current PALM-241 adaptive optics system, which comprise several flat mirrors and an off-axis parabola relay before the wavefront sensor. It is not expected that the relay for PALM-3000 will differ significantly in optical function or quality. Figure 4 show the spots diagrams for this model for each of the four microlens array configurations with the maximum spot sizes for each configuration presented in Table 3.

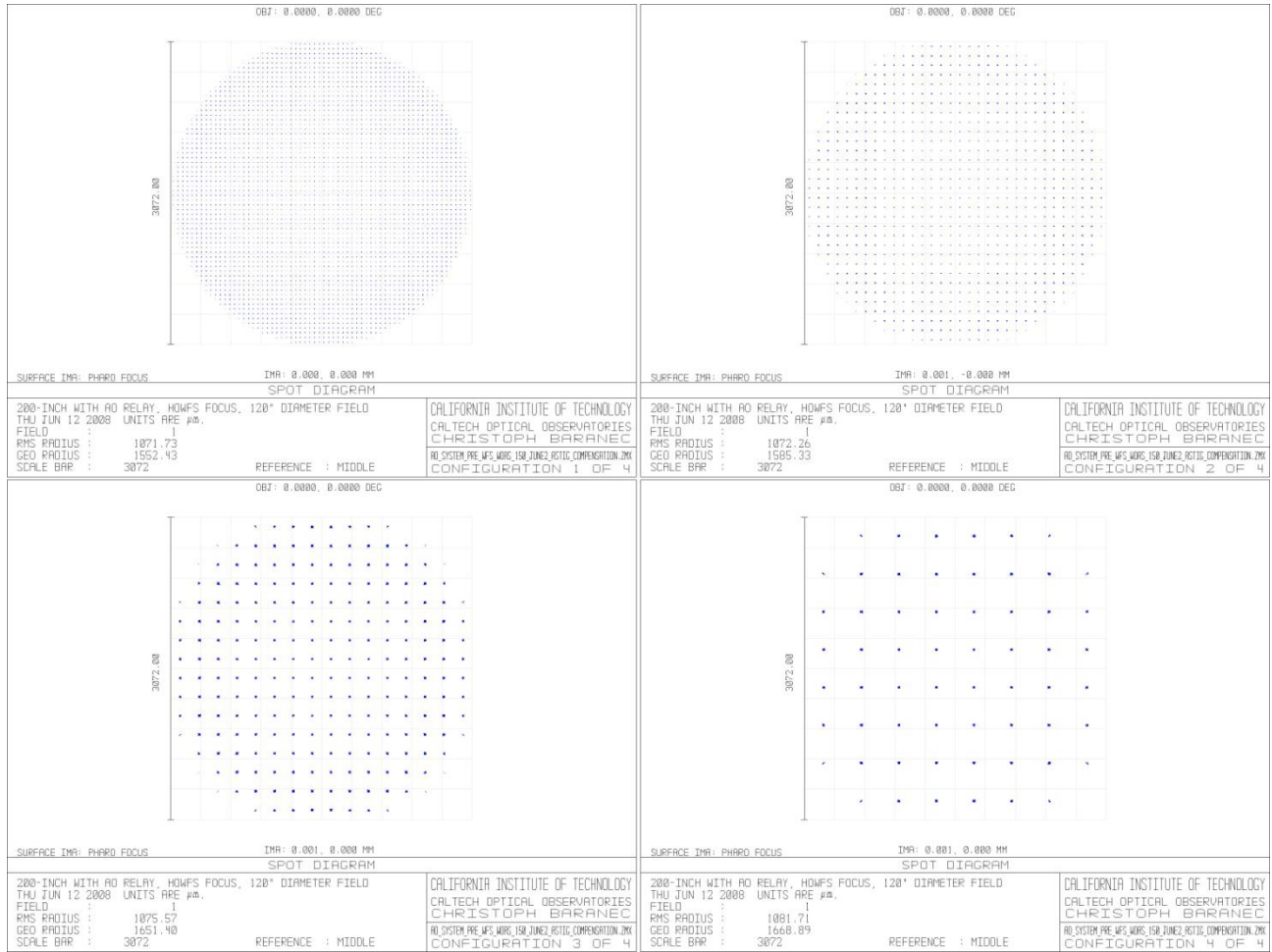


Fig. 4. Image plane spot diagrams for the high-order wavefront sensor system through the entire telescope and current PALM-241 optical system. Configurations for the $s = 64$ microlens array (upper left), $s = 32$ (upper right), $s = 16$ (lower left), and $s = 8$ (lower right).

Table 3. Maximum spot sizes in each Shack-Hartmann pattern for each microlens configuration. Angular size is calculated as the product of the RMS spot size and the plate scale chosen in Table 2.

| s | geometric (μm) | RMS (μm) | angular size (arc sec) |
|-----|--------------------------------|--------------------------|---------------------------|
| 64 | 9 | 4.6 | 0.40 |
| 32 | 13 | 5.1 | 0.32 |
| 16 | 18 | 9 | 0.48 |
| 8 | 21 | 10 | 0.27 |

The spot sizes are calculated assuming an even weighting to wavelengths over the wavelength range of $\lambda = 400 - 900$ nm, and are therefore expected to be smaller when the full λ -weighted quantum efficiency and source spectra are taken into account. In this case, imaging performance is on par with the original estimates assumed in Section 2.4 and is acceptable within the system's error budget.

3. MECHANICAL CONTROL

The high-order wavefront sensor includes many degrees of remote control. The whole sensor is mounted on a 150 mm linear stage to adjust for the differing focus of natural guide stars and the Sodium laser guide star. There is also a linear stage, with a minimum range of 12 mm, to which the detector and relay assemblies are attached which allows for change in focus when switching between different microlens arrays, and also allows for fine adjustment of the plate scale. The microlens arrays will be switched out by using a two axis stage which will also be used to register the microlenses to pixel boundaries. In addition, the adaptive optics bench will be equipped with a pair of mirrors with remote tip/tilt actuation which will be able to patrol a 2 arc minute field of view and will be used to center the guide star on the spatial filter and register the pupil location.

4. FUTURE WORK

With the design for the PALM-3000 high-order wavefront sensor now completed, it is expected that construction and testing will begin during the summer of 2008 and be finished by the fall. This will include further characterization of the CCD detector, procurement of hardware, alignment and integration of optics, testing of mechanical systems and initial wavefront measurement. Further study of the impact of matching geometry between the pupil projected on the deformable mirror actuators and the microlens arrays will be used to determine the best solution for the collimating element. Later this year, the high-order wavefront sensor will be integrated with the real-time wavefront controller²², which will calculate slopes and send commands to the two deformable mirrors. Full testing with optical feedback from the high-order deformable mirror will occur during integration of the entire adaptive optics system at Palomar in late 2009.

ACKNOWLEDGEMENTS

The author is grateful for support from the entire PALM-3000 team. This work has been supported by the National Science Foundation under grant AST-0619922, PI: Dr. R. Dekany.

REFERENCES

1. M. Troy, R. Dekany, G. Brack, B. Oppenheimer, E. Bloemhof, T. Trinh, F. Dekens, F. Shi, T. Hayward & B. Brandl, "Palomar adaptive optics project: status and performance," *Proc. SPIE Adaptive Optical Systems Technology*, ed. P. Wizinowich, **4007** (2000).
2. J. Roberts, A. Bouchez, J. Angione, R. Burruss, J. Cromer, R. Dekany, S. Guiwits, J. Henning, J. Hickey, E. Kibblewhite, D. McKenna, A. Moore, H. Petrie, J. C. Shelton, R. Thicksten, T. Trinh, R. Tripathi, M. Troy, T. Truong, & V. Velur, "Facilitizing the Palomar AO Laser Guide Star System," these proceedings.
3. T. L. Hayward, B. Brandl, B. Pirger, C. Blacken, G. E. Gull, J. Schoenwald & J. R. Houck, "PHARO: A Near-Infrared Camera for the Palomar Adaptive Optics System," *PASP*, **113**, 105-118 (2001).
4. N. Thatte, M. Tecza, F. Clarke, T. Goodsall, J. Lynn, D. Freeman & R. Davies, "The Oxford SWIFT integral field spectrograph," *Proc. SPIE Ground-based and Airborne Instrumentation for Astronomy*, eds. I. McLean & M. Iye, **6269** (2006).
5. S. Hinkley, B. Oppenheimer, D. Brenner, I. Parry, A. Sivaramkrishnan, R. Soummer & D. King, "A new integral field spectrograph for exoplanetary science at Palomar," these proceedings.
6. R. Dekany, A. Bouchez, M. Britton, V. Velur, M. Troy, J. C. Shelton & J. Roberts, "PALM-3000: Visible-light AO on the 5.1-meter Telescope," *Proc. SPIE Advances in Adaptive Optics II*, eds. B. Ellerbroek & D. B. Calia, **6272** (2006).
7. A. Bouchez, R. Dekany, J. Angione, C. Baranec, M. Britton, K. Bui, R. Burruss, J. Cromer, S. Guiwits, J. Henning, J. Hickey, D. McKenna, A. Moore, J. Roberts, T. Trinh, R. Tripathi, M. Troy, T. Truong & V. Velur, "The PALM-3000 high-order adaptive optics system for Palomar Observatory," these proceedings.
8. B. Macintosh, J. Graham, D. Palmer, R. Doyon, D. Gavel, J. Larkin, B. Oppenheimer, L. Saddlemyer, K. Wallace, B. Bauman, J. Evans, D. Erikson, K. Morzinski, D. Phillion, L. Poyneer, A. Sivaramkrishnan, R. Soummer, S. Thibault & J.-P. Veran, "The Gemini Planet Imager," *Proc. SPIE Advances in Adaptive Optics II*, eds. B. Ellerbroek & D. B. Calia, **6272** (2006).

9. T. Fusco, G. Rousset, J.-F. Sauvage, C. Petit, J.-L. Beuzit, K. Dohlen, D. Mouillet, J. Charton, M. Nicolle, M. Kasper, P. Baudoz & P. Puget, "High-order adaptive optics requirements for direct detection of extrasolar planets: Application to the SPHERE instrument," *Optics Express*, **14**, 7515-7534 (2006).
10. V. Velur, R. Flicker, R. Dekany, G. Rahmer, R. Smith & A. Moore, "Low-order wavefront sensing in tomographic multi-beacon adaptive optics systems," these proceedings.
11. L. Poyneer & B. Macintosh, "Spatially filtered wave-front sensor for high-order adaptive optics," *J. Opt. Soc. Am. A.*, **21**, 810-819 (2004).
12. E. Serabyn, K. Wallace, M. Troy, B. Mennesson, P. Haguenaer, R. Gappinger & R. Burruss, "Extreme Adaptive Optics Imaging with a Clear and Well-Corrected Off-Axis Telescope Subaperture," *ApJ*, **658**, 1386-1391 (2007).
13. F. Wildi, G. Brusa, A. Riccardi, R. Allen, M. Lloyd-Hart, D. Miller, B. Martin, R. Biasi & D. Gallieni, "Progress of the MMT adaptive optics program," *Proc. SPIE Adaptive Optics Systems and Technology II*, eds. R. Tyson, D. Bonaccini, & M. Roggemann, **4494** (2001).
14. Z. Hu & W. Jiang, "Optimum matching of wavefront sensor and wavefront corrector," *Proc. SPIE Adaptive Optical Systems and Applications*, eds. R. Tyson & R. Fugate, **2534** (1995).
15. A. Dubra, "Wavefront sensor and wavefront corrector matching in adaptive optics," *Optics Express*, **15**, 2762-2769 (2007).
16. W. Zou & J. P. Rolland, "Quantifications of error propagation in slope-based wavefront estimations," *JOSA A.*, **23**, 2629-2638 (2006).
17. J. R. P. Angel, "Ground-based imaging of extrasolar planets using adaptive optics," *Nature*, **368**, 203-207 (1994).
18. J. W. Hardy 1994, *Adaptive optics for astronomical telescopes*, (New York: Oxford University Press).
19. C. Baranec, "Concept for a Shack-Hartmann wavefront sensor with adjustable pupil sampling for astronomical adaptive optics," in preparation.
20. P. Feautrier, P. Kern, R. Dorn, G. Rousset, P. Rabou, S. Laurent, J.-L. Lizon, E. Stadler, Y. Magnard, O. Rondeaux, M. Cochard, D. Rabaud, A. Delboulbe, P. Puget & N. Hubin, "The NAOS visible wavefront sensor," *Proc. SPIE Adaptive Optical Systems Technology*, ed. P. Wizinowich, **4007** (2000).
21. G. Rousset, F. Lacombe, P. Puget, E. Gendron, R. Arsenault, P. Kern, D. Rabud, P.-Y. Madec, N. Hubin, G. Zins, E. Stadler, J. Charton, P. Gigan, P. Feautrier, "Status of the VLT Nasmyth Adaptive Optics System (NAOS)," *Proc. SPIE Adaptive Optical Systems Technology*, ed. P. Wizinowich, **4007** (2000).
22. T. Truong, T. Trinh, R. Dekany, A. Bouchez, J. Roberts, M. Troy & S. Guiwits, "Real-time wavefront control for the PALM-3000 high-order adaptive optics system," these proceedings.